Efficient sunlight driven CO_2 reduction on Graphene-wrapped Cu-Pt/rTiO$_2$ @ SiO$_2$

Mingyang Zhang [a], Muyan Wu [a], Zhenyu Wang [a,b], Rui Cheng [a], Dennis Y.C. Leung [a], Zhouguang Lu [b], Shien Ping Feng [a,*]

[a] Department of Mechanical Engineering, The University of Hong Kong, Pokfulam, Hong Kong
[b] Department of Materials Science and Engineering, Southern University of Science and Technology, China

A R T I C L E   I N F O

A B S T R A C T

The Photoreduction of CO_2 provides a promising way to solving environmental issues. In this work, hydrogen-doped Titania powders were fabricated using $NaBH_4$ heated with TiO_2 at 350 °C. The reduced Titania was decorated with Platinum nanoparticles by Poly (N-vinyl-2-pyrrolidone) PVP protected Pt solution. The copper precursor was mixed with the previous sample to get Cu-Pt bi-metal co-catalysts deposited on the surface of reduced TiO_2. After wrapping with graphene oxide (GO) sheets, core-shell-structured photocatalysts graphene-wrapped Cu-Pt/rTiO$_2$ be synthesized. A systematic study of CO_2 photoreduction performance of graphene-wrapped Cu-Pt/rTiO$_2$ was conducted using the on-line GC system with SiO$_2$ fiber as the substrate. Under AM1.5 G simulated sunlight, the graphene-wrapped Cu-Pt/rTiO$_2$ @ SiO$_2$ produced carbon monoxide (394.84 μmol g^{-1}cat 1. h^{-1}) from CO_2 with remarkable selectivity reaching 99%. Over 7 h of illumination period, the prepared sample was showing excellent stability with no decrease in origin CO_2 conversion rate. Elemental mapping and transmission electron microscopy images confirmed Cu-Pt bi-metal nanoparticles deposited on the surface of TiO_2 nanoparticles. The Inert gas control group test confirmed that carbon monoxide products originate from CO_2.

1. Introduction

In recent years, the increasing consumption of fossil fuels and the rising concentration of carbon dioxide in the atmosphere have caused severe environmental problems such as erratic weather patterns [1]. Because of the massive burning of fossil fuels, the current level of carbon dioxide far exceeds the natural fluctuations of the past 800,000 years, which is probably the highest in 1500 million years, according to the boron isotope ratio in plankton shells [2]. How to effectively reduce the carbon dioxide content in the atmosphere and make further use of it has become an important research topic all over the world. For more than three decades, researchers have tried to mimic the photosynthesis of plants in nature, which aims to spontaneously convert carbon dioxide and water from the atmosphere into chemical fuels, using sunlight as an energy input [3]. Among the various carbon dioxide reduction products, in terms of conversion and economic efficiency, CO has an absolute advantage in market compatibility and net present value [4,5]. Various semiconductor materials, such as CdS, g-C_3N_4, Fe_2O_3, Cu_2O, and WO_3, have been developed as active photocatalysts [6]. Because of its high reduction potential, low cost, and high stability, TiO_2 has attracted much attention as the most promising photocatalyst for carbon dioxide [7–9].

The most common crystalline phases of TiO_2 are rutile, anatase, and brookite. They all have large electronic bandgaps of 3.0–3.2 eV [10]. With such large bandgaps, titanium dioxide can only use ultraviolet light with a wavelength of fewer than 400 nm, which only accounts for 2–5% of the total spectrum. For carbon dioxide reduction, the ideal bandgap is estimated to be 1.8–2.0 eV. How to increase the light absorption of the semiconductor catalyst is the key to utilize solar energy effectively.

Doping is one of the commonly used techniques to extend the range of semiconductor optical absorption because it can effectively reduce the bandgap of the semiconductor. TiO_2 is treated

* Corresponding author.
E-mail address: hpfeng@hku.hk (S.P. Feng)

with a reducing agent to form an oxygen vacancy in the lattice, called the self-doping of TiO_2. Oxygen vacancy constitutes surface defects, which play an essential role in catalysis. It can alter the interaction between the surface of the catalyst and the target molecule, thus reducing the reaction activation energy and even changing the reaction pathway. Among the many experimental supports, scanning tunneling microscopy showed that carbon dioxide molecules were well absorbed in oxygen cavities. The quantum mechanical model also indicates that electron transfer from CB of stoichiometric anatase TiO_2 to CO_2 is not energetically favorable but defects on the surface of anatase TiO_2 can promote electron transfer to CO_2 [11]. Lin et al. reduced titanium dioxide with aluminum to obtain Titania with surface oxygen vacancy. Significant color changes in titanium dioxide can be observed. The white titanium dioxide before the reaction turns black after the reduction reaction. The non-metallic element X (X = H, N, S, I) was then added to the Al reduced titanium dioxide nanocrystals (TiO_{2-x}), resulting in the color change. All the TiO_{2-x} nanoparticles have enhanced absorption in the visible and near-infrared regions [12].

Depositing Metal Nano-particles on semiconductors is beneficial to the performance of photocatalysts. It can improve the charge separation, promote the activation of CO_2, and provide active catalytic sites for the reduction process. The Fermi levels of metal NPs are usually lower than the conduction band of TiO_2. The Schottky barrier can form at the interface between TiO_2 and metal NPs. The electrons produced by the light will then rapidly migrate from TiO_2 to the metal NPs through the Schottky barrier until their Fermi levels are equal [13]. For example, ultraviolet irradiation leads to a Fermi energy level equilibrium between TiO_2 and Au through charge distribution, thus causing the Fermi level shift –22 mV [14]. The Fermi level shift promotes the effective photocatalytic reaction and indicates the efficient electron transfer on the TiO_2 and metal NPs interface system. The commonly used metal nanoparticles as co-catalysts for TiO_2 are Pt, Pd, Cu, Ag, Ni, Co, and Au [15], etc. Using P25 TiO_2 powder as a base photocatalyst, Wang et al. showed that the ability of noble metal co-catalyst to promote CO_2 reduction is in the order of Ag < Rh < Au < Pd < Pt [16]. These metals can be used as electron sinks to concentrate photogenerated electrons produced by photocatalysts, thus reducing the possibility of electron-hole recombination [17].

Researches on bimetallic cocatalysts attracted exceptional attention. Numerous experiments have observed that copper and noble metals such as Pd, Pt, Au, Ag bimetallic catalysts can significantly improve the efficiency CO_2 photocatalytic conversion on semiconductors such as TiO_2 [18]. Strasser [19] and coworkers demonstrated that the compressive strain in the shell of Cu@Pt nanocrystals modified the d-band structure of the surface Pt atoms. The adsorption energy of the reaction intermediates diminished by this d band shift results in the bimetallic system superior to the undrained Pt catalyst [20].

Carbon nanomaterials such as carbon nanotubes and graphene Nano-sheets are widely used to improve TiO_2 photocatalytic reduction of CO_2, especially two-dimensional graphene. By loading of graphene can increase the specific surface area of photocatalyst, enhance the adsorption of carbon dioxide by π-π conjugation between CO_2 molecules and graphene, and accelerate the transportation of photo-generated electrons between photocatalyst particles due to its excellent conductivity [21]. Yilong Zhao and coworkers demonstrated that the thickness of reduced graphene oxide sheets could optimize the recombination rate of photogenerated charges. Where the sample contained 2% mass fraction rGO showed the optimum Photoluminescence spectra results [22].

The use of optical fibers as the support for photocatalysts can increase conversion rates when the optical fibers are simultaneously applied as a light distributing guide [23,24]. The high loading rate and the direct photoexcitation of the catalyst can achieve when coated on fibers. Quantz wool framed by SiO_2 threads practiced as a substrate can avoid agglomeration of powder samples and increases the reaction as well.

Herein, the core–shell-structured photocatalysts graphene-wrapped Cu-Pt/rTiO_2 be synthesized by a self-assembly method of a simple chemical bonding reactions and tested by coated on SiO_2 fibers as support. Under AM1.5 G simulated sunlight, the graphene-wrapped Cu-Pt/rTiO_2 @ SiO_2 produced carbon monoxide (400 μmol g^{-1}cat 1. h^{-1}) from CO_2 with remarkable selectivity reaching 99%. Over 7 h of illumination period, the prepared sample was showing excellent stability with no decrease in origin CO_2 conversion rate. Control group tests confirm the carbon monoxide products originate from CO_2.

2. Materials and methods

2.1. Materials

Titanium dioxide (Aeroxide® TiO_2 P25) procured from Evonik Degussa. Polyvinylpyrrolidone (PVP, average M.W.8000) provided by Acros Organics. Sodium Borohydride ($NaBH_4$ 98% purity) and Chloroplatinic acid hexahydrate ACS reagent (37.5% Pt basis) purchased from Sigma-Aldrich. Electroless copper plating solution ($CuSO_4 \cdot 5H_2O$ 7.6 g/L) purveyed by Haofan Technology Co., Ltd. Graphene Oxide Dispension (GO) obtained from Jining Leadernano Tech. L.L.C. High-temperature quartz fiber (99.99% purity, φ = 5 μ m, 2.2 g/cm³) acquired from Orris New Materials Technology Co., Ltd. High purity Nitrogen (99.99%), Carbon Dioxide (99.99%) and Helium (He, 99.99%) supplied by Linde HKG Ltd. The Millipore Direct Q-5 purification system-generated De-ionized water (DI water) exerted to prepare solutions and wash samples.

2.2. Sample preparation

Use a mortar and pestle to grind 200 mg of P25 with variable quantities of sodium borohydride, then place the mixtures in tube furnace heated under 350℃ for 30 min in the N_2 atmosphere to get reduced TiO_2 (rTiO_2).

The annealed samples were tested by Gas chromatography. rTiO_2 with the highest CO_2 reduction yield dispersed into DI water and dropped into PVP-Pt solution, and then put into ultrasonic sink for 30 min. Pt with a mass fraction of 0.35 wt% was introduced into the sample, the weight percentage calculated by platinum ionic concentration. The PVP-Pt solution is prepared by dissolving chloroplatinic acid precursor in water and reducing by sodium borohydride. PVP (Polyvinylpyrrolidone) operated as the dispersant.

A certain amount of electroless copper solution dropped into the sample, and the volume of the solution controlled by calculation, so that the mass fraction of copper introduced was 0.35 wt %. The graphene oxide (GO) aqueous suspension was then added to the sample in the same way, with a mass fraction of 2%. After 300 rpm stirring for 30 min, the samples were centrifuged to remove water and heat for 30 min at 350℃ in the tube furnace under N_2 flow. The prepared graphene-wrapped Cu-Pt/rTiO_2 powders were immobilized by dip-coating onto SiO_2 fibers. The sample preparation flow chart is shown in Fig. 1.

2.3. Characterization

As-prepared samples characterized by transmission electron microscopy (TEM) equipped with FEI Tecnai G2 20 S-TWIN. The morphology and elemental information obtained by high angle
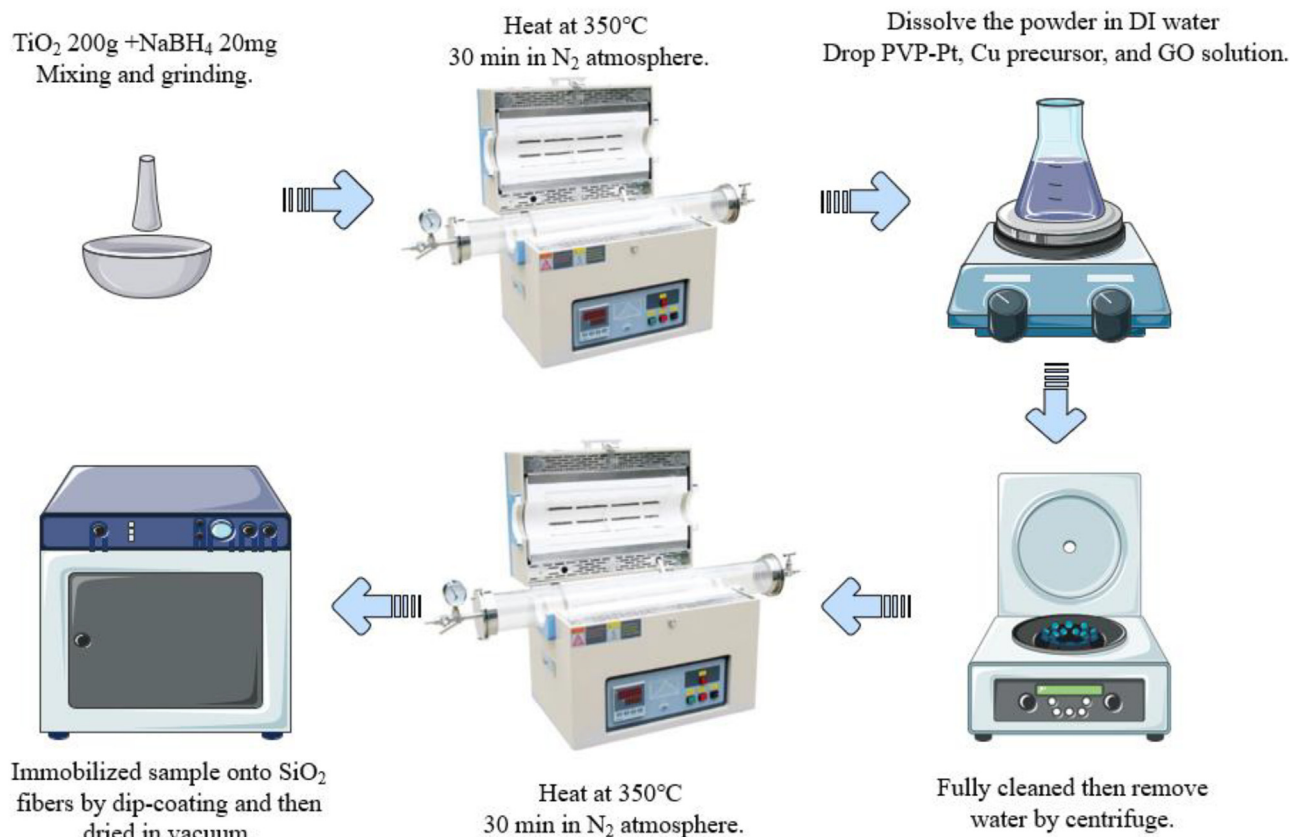
TiO₂ 200g +NaBH₄ 20mg
Mixing and grinding.

Heat at 350℃
30 min in N₂ atmosphere.

Dissolve the powder in DI water
Drop PVP-Pt, Cu precursor, and GO solution.

Immobilized sample onto SiO₂
fibers by dip-coating and then
dried in vacuum.

Heat at 350℃
30 min in N₂ atmosphere.

Fully cleaned then remove
water by centrifuge.

Fig. 1. Sample preparation flow chart.

annular dark-field (HAADF) scanning electron microscopy images and selected area electron diffraction (SAED), which was implemented in the transmission electron microscope (FEI Tecnai F30). UV–vis diffuse reflectance spectra (UV–vis DRS) detected on a Varian Cary 5000 Scan UV–Vis-NIR spectrometer with the reference of BaSO₄. High-accuracy mass flow controller (MFC YJ-700 Konxin) was exercised to control the flow rate of gas. Gas products analysis carried out by gas chromatography (GC, SRI instruments 8610C) equipped with helium ionization detector (HID) and thermal conductivity detector (TCD).

2.4. Photoreduction test

A 3 mg sample was dispersed on the SiO₂ fiber by dip-coating and placed in the center of the cylindrical reactor with a quartz window. Fill the reactor with the wet carbon dioxide and helium mixed gas with an airflow rate of 10 mL/min for 1 h. Then the reactor was placed under the sunlight simulator illuminated for 7 h under continuous airflow and the light intensity set to 1000 W/m² (AM 1.5G).

Under illumination, the gas in the reactor was injected into the gas chromatograph by continuous airflow with a rate of 10 mL/min. Ehsan Pipelzadeh and coworkers' research indicated that the disturbance of continuous gas flow is beneficial to adsorption and desorption. They compared constant pressure and press swing with gas flow and concluded that the photocatalytic efficiency is higher under the airflow [25]. GC detected the product concentration with a flame ionization detector (FID) and a thermal conductivity detector (TCD) each 60 min intervals. The gas products are analyzed by the external standard method.

Total CO yield (μmol)

$$CO yield(\mu mol) = \frac{(C_{final,CO} - C_{initial,CO}) \times Volumetric flow of product gas}{Amount of photocatalysts used(g)},$$ C_{CO} for concentration of CO

The Control group test was exercised with moist helium gas instead of CO_2/He mixture to determine the initial carbon products involved in the system.

3. Results and discussion

3.1. The characterization results of the catalysts

The sample was reduced by the variable amount of sodium borohydride at 350℃ under N₂ flow. The reduced titanium dioxide has shown in Fig. 2. With the NaBH₄ content increased, the samples' color went from white to dark, indicating that there were defects inside the titanium dioxide nanoparticles.

The UV–vis spectrum was shown in Fig. 3. The reduced titanium dioxide samples had significant light absorption in the visible area. This enhanced absorption is caused by a disordered surface and trivalent titanium ions. It is well known that hydrogen atoms in the amorphous layer can interact actively with Ti 3d and O 2p electrons, resulting in a significant reduction in the energy bandgap of the intermediate gap state [26]. Besides, hydrogenation causes surface states to be disordered, causing the maximum valence band to move upward, while Ti^{3+} and Vo make the conduction band minimum [27].

As the CO yield result shows in Fig. 3, the rTiO₂ generated by the reduction reaction of 200 mg P25 and 20 mg NaBH₄ shows the highest CO yield rate. During the detection process, no H₂ was detected. Tiny amounts of CH₄ were detected in samples with
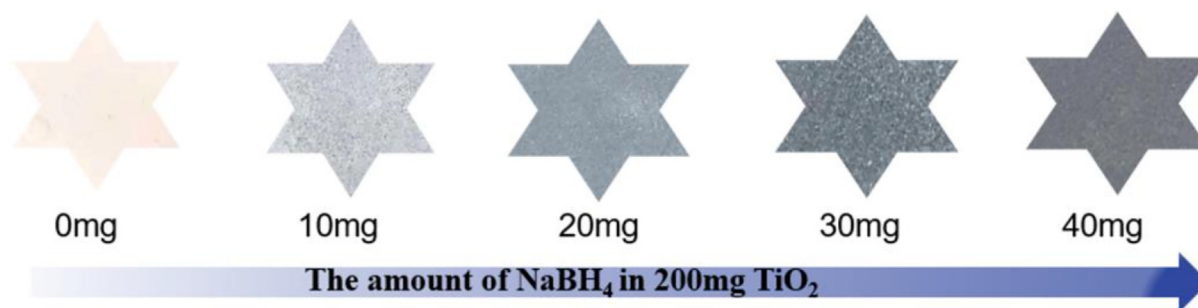
Fig. 2. Samples' color change to dark after the reduction concerning the amount of NaBH$_4$.

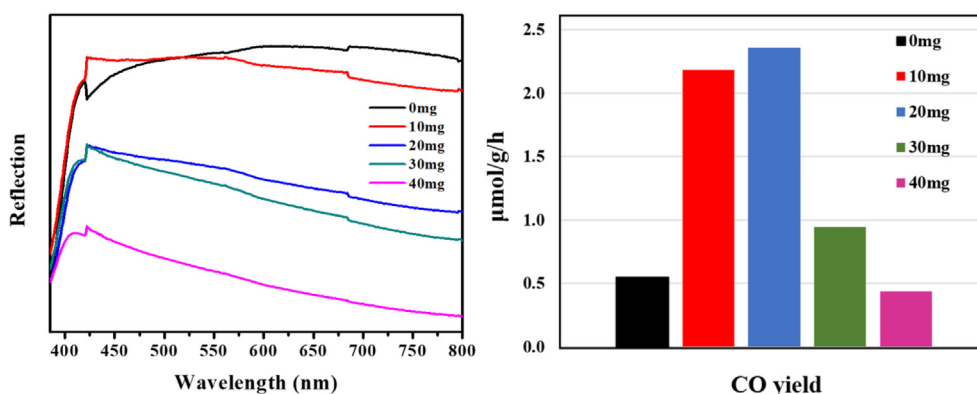Fig. 3. UV–vis DRS TiO2 reduced with different amount of NaBH4 and CO yield.

40 mg NaBH$_4$, but the overall reduction efficiency of the samples was still declined. Although light absorption becomes better with NaBH$_4$ continuously added in, the CO$_2$ reduction rate is not increasing. The results are consistent with works reported by others previously. Activity decline is most likely due to the recombine of photogenerated charges with excessive Ti^{3+} as recombination centers [28–30]. The rTiO$_2$ with the highest activity were used in subsequent preparation. Disperse this rTiO$_2$ into DI water, then combined with Cu-Pt nanoparticles and graphene oxide sheets to get the Graphene-wrapped Cu-Pt/ rTiO$_2$. No noticeable color change of those samples during the preparation steps.

The functional groups of the TiO$_2$, rTiO$_2$ unwashed, and rTiO$_2$ washed with DI water samples were identified by the Fourier transform infrared spectroscopy (FTIR). Fig. 4 (a) displays the IR KBr spectra for these three catalysts, while the spectral range was from 4000 to 400 cm^{-1}. The typical B-H bands (2200–2400 and 1125 cm^{-1}) are detectable by FTIR from unwashed rTiO$_2$. The

result proved the NaBH$_4$ residue in the sample after the reduction reaction, which could affect the photoreduction results due to hydrogen production. After thoroughly washing by DI water, the B-H disappeared, demonstrated that the rTiO$_2$ washed samples removed NaBH$_4$ impurities.

The effect of Cu composition on CO$_2$ photoconversion to CO yield is compared in Fig. 4 (b). The other components of the catalyst remain unchanged, and the CO$_2$ photoreduction rate decreases significantly after the mass fraction of copper was doubled. We can find the same trend in the experimental results of Saurav Sorcar and coworkers. For Pt-Cu bimetallic cocatalyst system, the surface of some Pt is exposed to the reaction gas and involved in the photocatalytic reaction rather than entirely covered by the Cu will lead to a better catalytic effect [31]. Due to the reaction mechanism of electroless copper plating, copper is targeted growth on the Pt surface. High copper content or low Pt content will result in a wholly covered Pt surface. They also displayed that with 0.35% mass fraction of Pt has an optimized effect, continuously increasing the
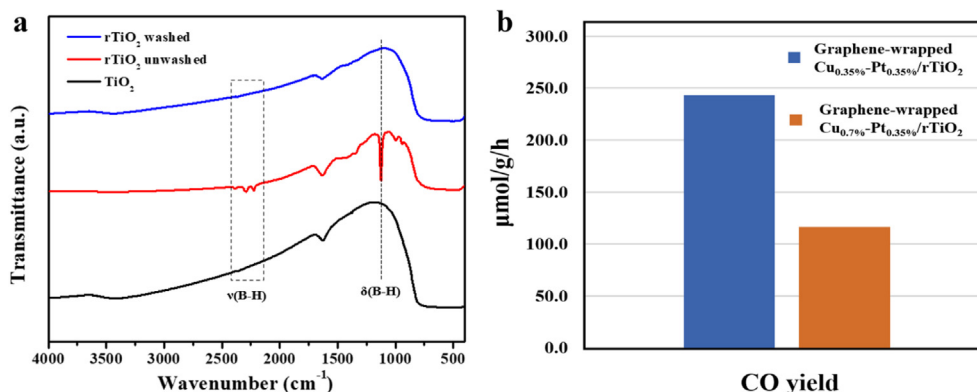

Fig. 4. (a) FTIR spectra of TiO$_2$, rTiO$_2$ unwashed and rTiO$_2$ washed catalysts, (b) Effect of Cu composition on CO$_2$ photoconversion to CO yield.

content of Pt will reduce the photocatalytic product. And this is consistent with Wei-Ning Wang and co-authors' work on the impact of Pt content and particle size for photocatalytic yield.

Increasing the mass fraction content of the Pt will cause the Pt nanoparticles aggregated into larger particle sizes. The size of Pt nanoparticles can significantly affect their work function, which will substantially affect the selectivity of photocatalysis. Wei-Ning Wang and co-authors demonstrated that as Pt nanoparticles become larger, their properties may be approaching that of bulk Pt, which could capture both photoelectrons and holes and act as recombination centers [32].

The high angle annular dark-field scanning transmission electron microscopy (HAADF) image and energy dispersive Xray spectroscopy (EDS) elemental mapping patterns for Ti, O, Pt, and Cu (Fig. 5**a, b, c, d, e, f**) endorsed that Pt and Cu nanoparticles are successfully decorated on rTiO$_2$.

The TEM images of the samples are showing in Fig. 5**g, h, i**. As can be seen in Fig. 5**g**, there is a typical cubic nanoparticle morphology of TiO$_2$ (P25) [33], with noticeable dark small particles deposited on the surface. The particles with sizes around 5 to 10 nm presented a non-uniformly shaded image in Fig. 5**h**. This phenomenon is often seen in TEM images of the nanoparticles formed by different metals [34,35]. The lattice deformation that appears in Fig. 5**i** supports the formation of this nanoparticle by different kinds of minerals [36–38]. Combined lattice structure with the EDS elemental mapping results, it indicated that this nanoparticle is a Cu-Pt bimetallic particle.

3.2. Photocatalytic activity for CO$_2$ reduction and discussion

The stainless steel reactor used in the gas chromatographic analysis is shown in Fig. 6 **(a)**. The UV–visible diffuse reflectance
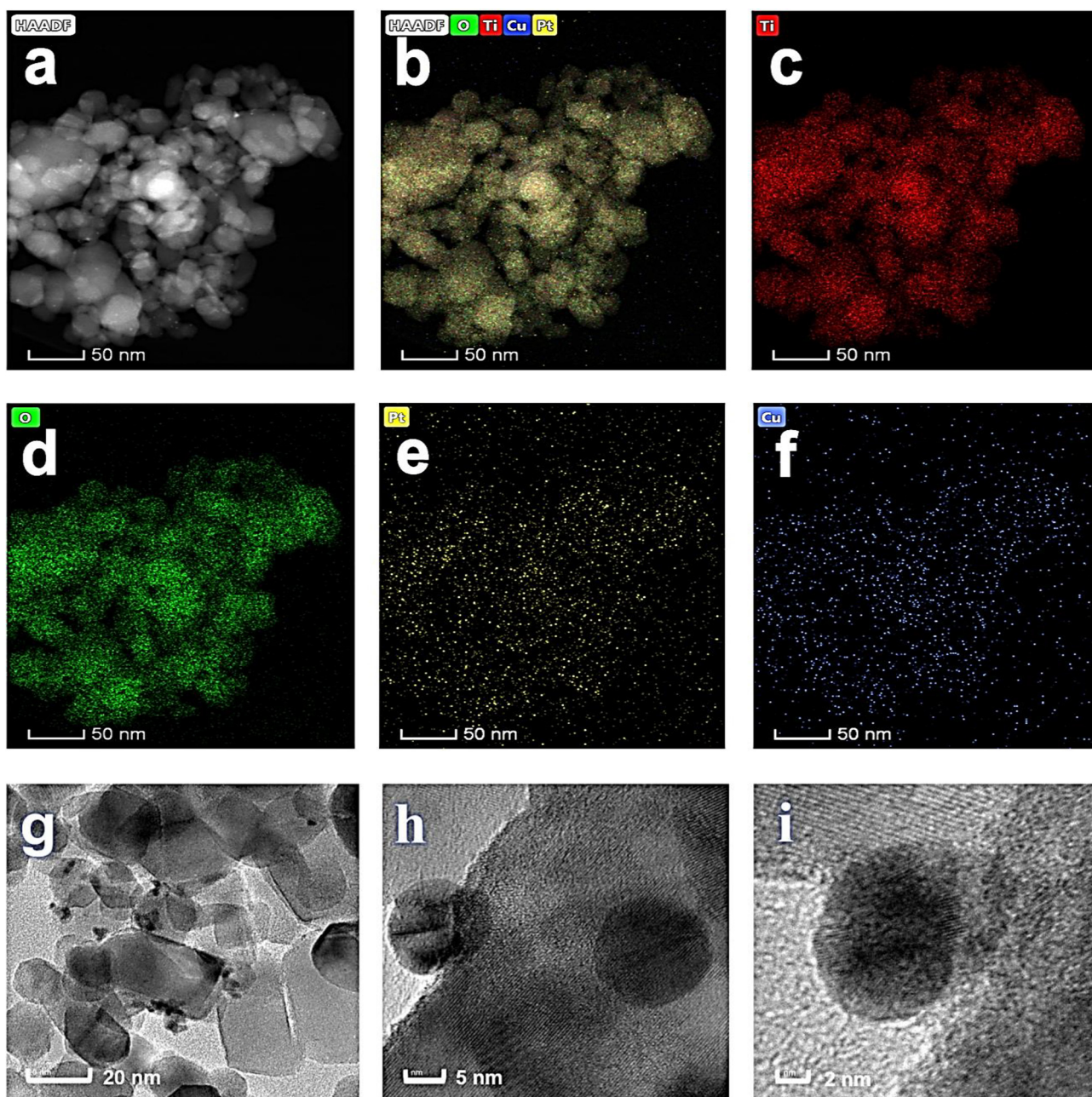
Fig. 5. (a) (b) annular dark-field scanning transmission microscope (HAADF-STEM) image and energy dispersive X-ray spectroscopy (EDS) mapping of the (c)Ti, (d) O, (e) Pt, and (f) Cu, respectively, of the Cu-Pt/rTiO$_2$ nanocomposites (g) (h) (i) transmission electron microscopy (TEM) images of the graphene-wrapped Cu-Pt/rTiO$_2$ nanocomposites.
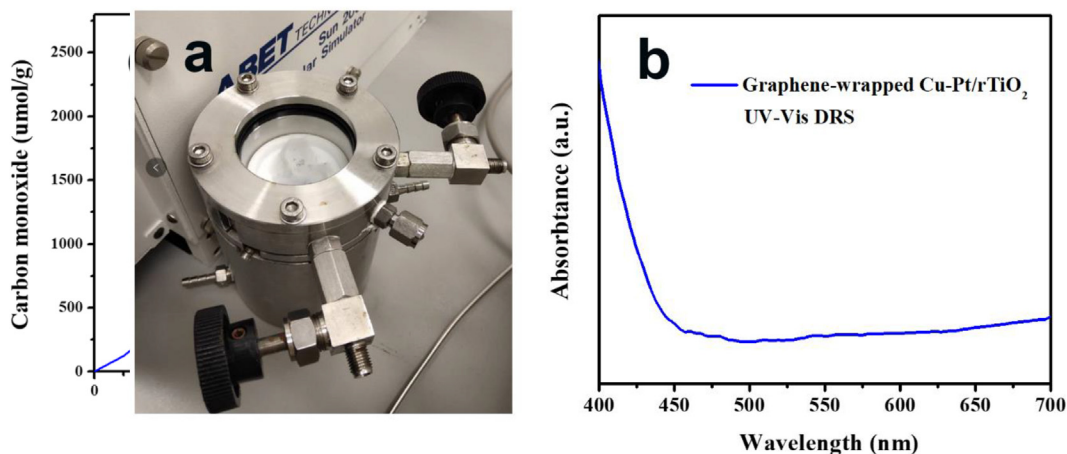
Fig. 6. (a) Stainless steel reactor, (b) UV–vis DRS of graphene-wrapped Cu-Pt/rTiO$_2$, (c) (d) Production results from GC.

spectra of graphene-wrapped Cu-Pt/rTiO$_2$ are presented in Fig. 6 **(b).** The light absorption of 450–500 nm is observed. A systematic study of CO$_2$ photoreduction performance of graphene-wrapped Cu-Pt/rTiO$_2$ was conducted using the on-line GC system with SiO$_2$ fiber as the substrate. Under AM1.5 G simulated sunlight, the graphene-wrapped Cu-Pt/rTiO$_2$ @ SiO$_2$ produced carbon monoxide (394.84 μmol g^{-1}cat 1. h^{-1}) from CO$_2$ with remarkable selectivity reaching 99%. Over 7 h of illumination period, the prepared sample was showing excellent stability with no decrease in origin CO$_2$ conversion rate, the results displayed in Fig. 6 **(c) (d)**.

Total CO yield (μmol)

$$COyield(\mu mol) = \frac{(C_{final,CO} - C_{initial,CO}) \times Volumetricflowofproductgas}{Amountofphotocatalystsused(g)}$$, C$_{CO}$ for concentration of CO

The N$_2$ adsorption isotherms characterized the BET surface area (SBET) and pore volume of the graphene-wrapped Cu-Pt/rTiO$_2$ and graphene-wrapped Cu-Pt/rTiO$_2$ @ SiO$_2$ catalysts displayed in Fig. 7. The BET surface areas of graphene-wrapped Cu-Pt/rTiO$_2$ and graphene-wrapped Cu-Pt/rTiO$_2$ @ SiO$_2$ are 57.034 m^2 g^{-1}and 97.366 cm^2 g^{-1}, respectively (Table 1).

The sample coated on SiO$_2$ fiber has a larger surface area due to the 3 D (3 dimensions) structure formed by the fibers. The properties such as external surface area and light transmittance of the optical fibers were reported to have a positive effect on photoconversion of the catalysts [23]. The 3 D structure of the SiO$_2$ fiber increases the surface area of the powder catalyst not only exposed more reactive active sites but also more favorable for the adsorption and desorption of reactants and products. Moreover, fiber

Table 1
Comparison of physicochemical properties of different catalysts.

Sample	Surface area (m^2/g)	Pore volume (cm^3/g)	Pore diameter Dv(d) (nm)
Graphene-wrapped Cu-Pt/rTiO$_2$	57.034	0.501	3.820
Graphene-wrapped Cu-Pt/rTiO$_2$ @ SiO$_2$	97.366	0.155	3.052

could work as a channel of light transmission. Light gets into the SiO$_2$ fiber can be transmitted along with the core to the tail, which significantly improves the light absorption of the underlying catalyst and benefits the photoconversion efficiency.

Although a small amount of powder samples is advantageous in calculating the yield per gram, the absorption efficiency of light is low. On the other hand, redundant samples coating on the SiO$_2$ will cause the powder to fall off, so it no longer has the advantage of the enlarged surface area of the 3 D structure and the upper layer block the lower layer of illumination will reduce the photocatalytic yield. Therefore, in the test process using a coating on the SiO$_2$ surface without shedding samples.

3.3. Apparent quantum yield (AQY) calculation

Apparent quantum yield (AQY) is calculated by the equation below [31]

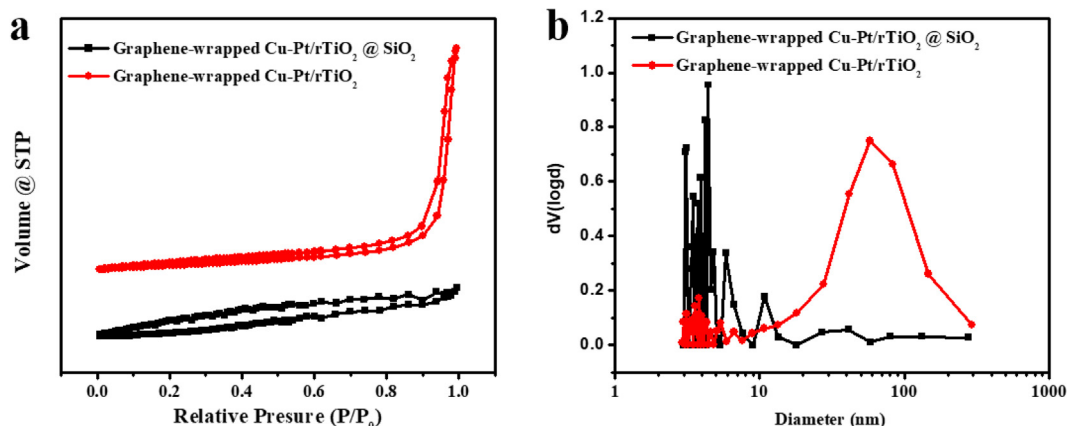AQY (%)$= \frac{Numberofreactedelectrons}{Numberofincidentphotons} \times 100$

Fig. 7. (a) N$_2$ adsorption isotherms, (b) BJH pore site distribution of graphene-wrapped Cu-Pt/rTiO$_2$ and graphene-wrapped Cu-Pt/rTiO$_2$ @ SiO$_2$ catalysts.

The AQY values for CO evolution of CO_2 reduction were calculated according to the following equation:

$$AQY(\%) = \frac{2 \times Number\,of\,evolved\,CO\,moleculars}{Number\,of\,incident\,photons} \times 100$$

Graphene-wrapped Cu-Pt/$rTiO_2$ @ SiO_2 produced carbon monoxide (394.84 μmol g^{-1}cat 1. h^{-1}), the number of reacted electrons is 4.755×10^{20}

Number of incident photons $= \frac{Light\,absorbed\,by\,the\,photocatalyst}{The\,average\,photon\,energy} \times t$, t is the time (s)

Light absorbed by the photocatalyst = H $\times$ A = 0.314 J/s, H = 100 mW/cm^2, A is reactor irradiation area.

The average photon energy $= \frac{hc}{\lambda} = 5.64 \times 10^{-19}$ J

Number of incident photons $= 2 \times 10^{21}$ J

AQY(%) of graphene-wrapped Cu-Pt/$rTiO_2$ @ SiO_2 sample is 23.77%.

4. Conclusions

In summary, core-shell-structured photocatalysts graphene-wrapped Cu-Pt/$rTiO_2$ @ SiO_2 with high activity and stability were synthesized by an economical method for efficient photoreduction of CO_2. The graphene-wrapped Cu-Pt/$rTiO_2$ @ SiO_2 not only achieved a remarkable CO_2 photoreduction performance with excellent activity and stability but also demonstrated a controllable, economical, and can be large-scale industrialized preparation process. The developed fabrication process was solution-processed, highly controllable, and environmentally-friendly. In brief, the highly efficient and stable graphene-wrapped Cu-Pt/$rTiO_2$ @ SiO_2 shows a potential of industrial-scale CO production and demonstrates a way of waste light utilization.

Disclosures

The authors declare no competing financial interests. M.Z. and S.P.F. developed the concept and designed the experiments. M.Z., M.W., and D. Y. C. L. contributed to perform the experiments. M.Z., Z.W., and Z.G.L. contributed to the material characterizations. M.Z., R.C., and S.P.F. contributed to the interpretation of the results. M.Z. and S.P.F. co-wrote the manuscript.

Declaration of Competing Interest

The authors declare that they have no known competing financial interests or personal relationships that could have appeared to influence the work reported in this paper.

Acknowledgments

References

[1] S.J. Davis, K. Caldeira, H.D. Matthews, Future CO2 emissions and climate change from existing energy infrastructure, Science 329 (2010) 1330–1333.

[2] P.N. Pearson, M.R. Palmer, Atmospheric carbon dioxide concentrations over the past 60 million years, Nature 406 (2000) 695.

[3] S. Chu, Y. Cui, N. Liu, The path towards sustainable energy, Nat. Mater. 16 (2017) 16–22.

[4] M. Jouny, W. Luc, F. Jiao, General techno-economic analysis of CO2 electrolysis systems, Ind. Eng. Chem. Res. 57 (2018) 2165–2177.

[5] J. Chen, Z. Wang, H. Lee, J. Mao, C.A. Grimes, C. Liu, M. Zhang, Z. Lu, Y. Chen, S.-P. Feng, Efficient electroreduction of CO2 to CO by Ag decorated S-doped g-C3N4/CNT nanocomposites at industrial-scale current density, Mater. Today Phys. (2020) 100176.

[6] A. Priya, R. Senthil, A. Selvi, P. Arunachalam, C.S. Kumar, J. Madhavan, R. Boddula, R. Pothu, A.M. Al-Mayouf, A study of photocatalytic and photoelectrochemical activity of as-synthesized WO3/g-C3N4 composite photocatalysts for AO7 degradation, Mater. Sci. Energy Technol. 3 (2020) 43–50.

[7] T. Kamegawa, N. Suzuki, H. Yamashita, Design of macroporous TiO 2 thin film photocatalysts with enhanced photofunctional properties, Energy Environ. Sci. 4 (2011) 1411–1416.

[8] Y. Ma, X. Wang, Y. Jia, X. Chen, H. Han, C. Li, Titanium dioxide-based nanomaterials for photocatalytic fuel generations, Chem. Rev. 114 (2014) 9987–10043.

[9] Z. Bian, J. Zhu, J. Wen, F. Cao, Y. Huo, X. Qian, Y. Cao, M. Shen, H. Li, Y. Lu, Single-crystal-like titania mesocages, Angew. Chem. Int. Ed. 50 (2011) 1105–1108.

[10] O. Carp, C.L. Huisman, A. Reller, Photoinduced reactivity of titanium dioxide, Prog. Solid State Chem. 32 (2004) 33–177.

[11] V.P. Indrakanti, H.H. Schobert, J.D. Kubicki, Quantum mechanical modeling of CO2 interactions with irradiated stoichiometric and oxygen-deficient anatase TiO2 surfaces: implications for the photocatalytic reduction of CO2, Energy Fuels 23 (2009) 5247–5256.

[12] T. Lin, C. Yang, Z. Wang, H. Yin, X. Lü, F. Huang, J. Lin, X. Xie, M. Jiang, Effective nonmetal incorporation in black titania with enhanced solar energy utilization, Energy Environ. Sci. 7 (2014) 967–972.

[13] J. Low, B. Cheng, J. Yu, Surface modification and enhanced photocatalytic CO2 reduction performance of TiO2: a review, Appl. Surf. Sci. 392 (2017) 658–686.

[14] V. Subramanian, E.E. Wolf, P.V.J.J.o.t.A.C.S. Kamat, Catalysis with TiO2/gold nanocomposites. Effect of metal particle size on the Fermi level equilibration, 126 (2004) 4943-4950.

[15] K. Bhardwaj, A. Jaiswal, Fabricating gold nanorattles impregnated chitosan film for catalytic application, Mater. Sci. Energy Technol. 3 (2020) 167–173.

[16] S. Xie, Y. Wang, Q. Zhang, W. Deng, Y.J.A.C. Wang, MgO-and Pt-promoted TiO2 as an efficient photocatalyst for the preferential reduction of carbon dioxide in the presence of water, 4 (2014) 3644-3653.

[17] J. Yang, D. Wang, H. Han, C.J.A.o.c.r. Li, Roles of cocatalysts in photocatalysis and photoelectrocatalysis, 46 (2013) 1900-1909.

[18] Q. Zhai, S. Xie, W. Fan, Q. Zhang, Y. Wang, W. Deng, Y. Wang, Photocatalytic conversion of carbon dioxide with water into methane: platinum and copper (I) oxide co-catalysts with a core–shell structure, Angew. Chem. Int. Ed. 52 (2013) 5776–5779.

[19] P. Strasser, S. Koh, T. Anniyev, J. Greeley, K. More, C. Yu, Z. Liu, S. Kaya, D. Nordlund, H. Ogasawara, Lattice-strain control of the activity in dealloyed core–shell fuel cell catalysts, Nat. Chem. 2 (2010) 454.

[20] K.D. Gilroy, A. Ruditskiy, H.-C. Peng, D. Qin, Y. Xia, Bimetallic nanocrystals: syntheses, properties, and applications, Chem. Rev. 116 (2016) 10414–10472.

[21] S.C. Cui, X.Z. Sun, J.G.J.C. Liu, Photo-reduction of CO2 Using a Rhenium Complex Covalently Supported on a Graphene/TiO2, Composite 9 (2016) 1698–1703.

[22] Y. Zhao, Y. Wei, X. Wu, H. Zheng, Z. Zhao, J. Liu, J. Li, Graphene-wrapped Pt/ TiO2 photocatalysts with enhanced photogenerated charges separation and reactant adsorption for high selective photoreduction of CO2 to CH4, Appl. Catal. B 226 (2018) 360–372.

[23] O. Ola, M.M. Maroto-Valer, Review of material design and reactor engineering on TiO2 photocatalysis for CO2 reduction, J. Photochem. Photobiol., C 24 (2015) 16–42.

[24] J. Xu, Y. Ao, D. Fu, Y. Lin, X. Shen, C. Yuan, Z. Yin, Photocatalytic activity on TiO2-coated side-glowing optical fiber reactor under solar light, J. Photochem. Photobiol., A 199 (2008) 165–169.

[25] E. Pipelzadeh, V. Rudolph, G. Hanson, C. Noble, L. Wang, Photoreduction of CO2 on ZIF-8/TiO2 nanocomposites in a gaseous photoreactor under pressure swing, Appl. Catal. B 218 (2017) 672–678.

[26] R. Fu, S. Gao, H. Xu, Q. Wang, Z. Wang, B. Huang, Y.J.R.A. Dai, Fabrication of Ti 3 + self-doped TiO 2 (A) nanoparticle/TiO 2 (R) nanorod heterojunctions with enhanced visible-light-driven photocatalytic properties, 4 (2014) 37061-37069.

[27] Z. Wang, C. Yang, T. Lin, H. Yin, P. Chen, D. Wan, F. Xu, F. Huang, J. Lin, X.J.A.F.M. Xie, H-doped black titania with very high solar absorption and excellent photocatalysis enhanced by localized surface plasmon resonance, 23 (2013) 5444-5450.

[28] Z. Wang, C. Yang, T. Lin, H. Yin, P. Chen, D. Wan, F. Xu, F. Huang, J. Lin, X. Xie, H-doped black titania with very high solar absorption and excellent photocatalysis enhanced by localized surface plasmon resonance, Adv. Funct. Mater. 23 (2013) 5444–5450.

[29] A. Razzaq, A. Sinhamahapatra, T.-H. Kang, C.A. Grimes, J.-S. Yu, S.-I. In, Efficient solar light photoreduction of CO2 to hydrocarbon fuels via magnesiothermally reduced TiO2 photocatalyst, Appl. Catal. B 215 (2017) 28–35.

[30] A. Sinhamahapatra, J.-P. Jeon, J.-S. Yu, A new approach to prepare highly active and stable black titania for visible light-assisted hydrogen production, Energy Environ. Sci. 8 (2015) 3539–3544.

[31] S. Sorcar, Y. Hwang, J. Lee, H. Kim, K.M. Grimes, C.A. Grimes, J.-W. Jung, C.-H. Cho, T. Majima, M.R. Hoffmann, CO 2, water, and sunlight to hydrocarbon fuels: a sustained sunlight to fuel (Joule-to-Joule) photoconversion efficiency of 1%, Energy Environ. Sci. 12 (2019) 2685–2696.

[32] W.-N. Wang, W.-J. An, B. Ramalingam, S. Mukherjee, D.M. Niedzwiedzki, S. Gangopadhyay, P. Biswas, Size and structure matter: enhanced CO2

photoreduction efficiency by size-resolved ultrafine Pt nanoparticles on TiO2 single crystals, J. Am. Chem. Soc. 134 (2012) 11276–11281.

[33] X. Jiang, M. Manawan, T. Feng, R. Qian, T. Zhao, G. Zhou, F. Kong, Q. Wang, S. Dai, J.H. Pan, Anatase and rutile in evonik aeroxide P25: Heterojunctioned or individual nanoparticles?, Catal. Today 300 (2018) 12–17.

[34] W. Long, P. Liu, Y. Lv, W. Xiong, F. Hao, H.a. Luo,, Silica-supported Cu–Pt bimetallic catalysts for liquid-phase diethyl oxalate hydrogenation, Can. J. Chem. 96 (2018) 394–403.

[35] S. Mandegarzad, J.B. Raoof, S.R. Hosseini, R. Ojani, Cu-Pt bimetallic nanoparticles supported metal organic framework-derived nanoporous carbon as a catalyst for hydrogen evolution reaction, Electrochim. Acta 190 (2016) 729–736.

[36] X. Long, P. Yin, T. Lei, K. Wang, Z. Zhan, Methanol electro-oxidation on Cu@ Pt/ C core-shell catalyst derived from Cu-MOF, Appl. Catal. B 260 (2020) 118187.

[37] L. Deng, M.T. Nguyen, S. Mei, T. Tokunaga, M. Kudo, S. Matsumura, T. Yonezawa, Preparation and growth mechanism of Pt/Cu alloy nanoparticles by sputter deposition onto a liquid polymer, Langmuir 35 (2019) 8418–8427.

[38] J. Liu, M. Liu, X. Yang, H. Chen, S.F. Liu, J. Yan, Photo-redeposition synthesis of bimetal Pt–Cu Co-catalysts for TiO2 photocatalytic solar-fuel production, ACS Sustainable Chem. Eng. 8 (2020) 6055–6064.